Journal of Magnetic Resonance 200 (2009) 189–197

Contents lists available at ScienceDirect

Journal of Magnetic Resonance

journal homepage: www.elsevier.com/locate/jmr

Quantitative characterization of tissue microstructure with temporal diffusion spectroscopy ☆

Junzhong Xu [a,b,*], Mark D. Does [a,b,c,d], John C. Gore [a,b,c,e,f]

[a] Institute of Imaging Science, Vanderbilt University, Nashville, TN 37232, USA
[b] Department of Radiology and Radiological Sciences, Vanderbilt University, Nashville, TN 37232, USA
[c] Department of Biomedical Engineering, Vanderbilt University, Nashville, TN 37232, USA
[d] Department of Electrical Engineering, Vanderbilt University, Nashville, TN 37232, USA
[e] Department of Physics and Astronomy, Vanderbilt University, Nashville, TN 37232, USA
[f] Department of Molecular Physiology and Biophysics, Vanderbilt University, Nashville, TN 37232, USA

ARTICLE INFO

Article history:
Received 30 January 2009
Revised 26 June 2009
Available online 3 July 2009

Keywords:
Temporal diffusion spectroscopy
Oscillating gradient
Diffusion time
Simulation
Modeling

ABSTRACT

The signals recorded by diffusion-weighted magnetic resonance imaging (DWI) are dependent on the micro-structural properties of biological tissues, so it is possible to obtain quantitative structural information non-invasively from such measurements. Oscillating gradient spin echo (OGSE) methods have the ability to probe the behavior of water diffusion over different time scales and the potential to detect variations in intracellular structure. To assist in the interpretation of OGSE data, analytical expressions have been derived for diffusion-weighted signals with OGSE methods for restricted diffusion in some typical structures, including parallel planes, cylinders and spheres, using the theory of temporal diffusion spectroscopy. These analytical predictions have been confirmed with computer simulations. These expressions suggest how OGSE signals from biological tissues should be analyzed to characterize tissue microstructure, including how to estimate cell nuclear sizes. This approach provides a model to interpret diffusion data obtained from OGSE measurements that can be used for applications such as monitoring tumor response to treatment *in vivo*.

1. Introduction

Measurements of tissue structure over different distance scales may be important in both clinical and research applications. For example, the size of axons reflects structure in white matter and the conduction velocity of myelinated neurons varies roughly linearly with axon diameter [1–3]. Similarly, it has been reported that rates of cell division may be closely related to cell size. For some cells, there is a mechanism by which cell division is not initiated until a cell has reached a certain size [4] while measurements of tumor cell nuclear size have been suggested as a biomarker for tumor detection and grading [5,6]. Usually, histological information may be obtained only from invasive biopsies. However, diffusion-weighted (DW) magnetic resonance imaging is dependent on specific micro-structural properties of biological tissues, so it may be possible to obtain quantitative structural information non-invasively from DWI measurements. Diffusion in tissues is slower than in free solutions because tissue compartments hinder or restrict fluid motions, and the reduction in diffusion rates reflects the scale and nature of the tissue environment.

Stejskal suggested the use of a conditional probability approach to describe restricted diffusion analytically [7] and this approach enables an averaged diffusion propagator to be used to reveal dynamic displacements of water molecules in a certain diffusion time in q-space [8]. Cory used this method to demonstrate that the size of a diffusion compartment can be obtained from appropriate diffusion NMR experiments [9]. Others have derived the analytical conditional probability functions and signal attenuation dependence of diffusion within some simple geometries, such as diffusion between two infinitely large impermeable planes, or inside an infinitely long impermeable cylinder or an impermeable sphere [10–12]. Neuman modeled DW signals with a constant field gradient [13] and based on this analysis, Assaf et al. developed an AxCaliber model to obtain the diameter distribution of nerve axons [3]. Similarly, Zhao et al. estimated HeLa cell sizes [14] based on a statistical model [15] and the analytical root mean square (rms) displacement in a sphere at long diffusion times. All of these approaches are based on measurements using the pulsed gradient spin echo (PGSE) method with assumptions of short-gradient durations and/or long diffusion times. However, in

☆ Grant support: NIH CA109106, NS034834, EB001744 and NSF 0448915.
* Corresponding author. Address: Vanderbilt University, Institute of Imaging Science, 1161 21st Avenue South, AA 1105 MCN, Nashville, TN 37232-2310, USA. Fax: +1 615 322 0734.
E-mail address: junzhong.xu@vanderbilt.edu (J. Xu).

1090-7807/$ - see front matter © 2009 Elsevier Inc. All rights reserved.
doi:10.1016/j.jmr.2009.06.022

practice, the finite duration of gradients may invalidate the short gradient approximation. More importantly, conventional PGSE methods are insensitive to relatively short distance scales, such as those that characterize intracellular structures, because they incorporate relatively long diffusion times necessitated by hardware limitations. By contrast, oscillating gradient spin echo (OGSE) methods at high frequencies can probe short diffusion times and, hence, have the potential to detect changes over much shorter length scales [16]. The OGSE method has been successfully implemented experimentally to probe structural information including short length scales in packed beads [17], *in vivo* in ischemic rat brain [18], to study hyperpolarized gas diffusion [19] and to characterize tumors [20]. However, due to the relatively complicated gradient waveforms used in the OGSE method, analytical descriptions of DW signals with OGSE have not previously been reported. An appropriate model would be useful in order to interpret DW data obtained from OGSE measurements quantitatively.

Callaghan developed a simple matrix formalism to analyze restricted diffusion with generalized diffusion gradient waveforms quasi-analytically [21]. This approach discretizes the waveforms into many short pulses and calculates the MR signal attenuation recursively. However, it does not provide a simple analytical expression to describe the explicit relation of MR signals and tissue parameters. A frequency-domain analysis, which we have termed temporal diffusion spectroscopy [22], was originally introduced by Stepisnik [23,24]. Using a Gaussian approximation for the phase distribution, this analysis shows the DW signal attenuation is dependent on temporal auto-correlation function of the water molecule velocity at short diffusion scales. The frequency-domain analysis explicitly identifies the diffusion coefficient as a function of the frequency spectral content of the molecular velocity and reveals the relation between the choice of gradient waveforms and effective diffusion times [25]. In the present work, we build on these ideas and derive explicit analytical expressions for the DW echo signal attenuation for two commonly used OGSE methods, employing sine-modulated and cosine-modulated waveforms, respectively, for specific structures with known conditional probabilities. Based on the derived analytical equations, we have fitted simulated diffusion data in two model tissues (mimicking white matter and tumor) in order to show how quantitative tissue structural information, such as axon size and cell nuclear size, can be extracted. These results suggest how experimental OGSE data should be fitted and interpreted. The limitation of our model and the influence of the signal-to-noise ratios (SNR) of experimental measurements were also investigated.

2. Theory

2.1. Temporal diffusion spectroscopy with restricted diffusion

It has been previously shown that the DW echo signal attenuation can be described as [24]

$$E(2\tau) = \exp[-\beta(2\tau)] = \exp\left\{-\frac{\gamma^2}{2}\int_0^{2\tau} dt_1 \int_0^{2\tau} dt_2 \mathbf{g}(t_1)\langle \mathbf{r}_1(t_1)\mathbf{r}_2(t_2)\rangle \mathbf{g}(t_2)\right\}, \quad (1)$$

where β = the signal echo attenuation, τ = half of the echo time, $\mathbf{r}$ = the water molecule position, $\mathbf{g}$ = diffusion gradient and $\langle\ \rangle$ denotes the ensemble average. With the presence of diffusion restrictions, a conditional probability P may be introduced, which can be expressed in a general solution as [26]

$$P(\mathbf{r}_1, t_1|\mathbf{r}_2, t_2) = \sum_n \exp(-\lambda_n D|t_1 - t_2|) u_n(\mathbf{r}_1) u_n^*(\mathbf{r}_2), \quad (2)$$

where the $u_n(\mathbf{r})$ are orthogonal functions dependent on geometries. By substituting Eq. (2) into Eq. (1) as shown below, Stepisnik obtained the signal echo attenuation [24]

$$\begin{aligned}\beta(2\tau) &= \frac{\gamma^2}{2}\int_0^{2\tau} dt_1 \int_0^{2\tau} dt_2 \int_V d\mathbf{r}_1 \\ &\quad \times \int_V d\mathbf{r}_2 \rho(\mathbf{r}_1, t_1) P(\mathbf{r}_1, t_1|\mathbf{r}_2, t_2)\mathbf{r}_1\mathbf{g}(t_1)\mathbf{r}_2\mathbf{g}(t_2) \\ &= \frac{\gamma^2}{2}\sum_n B_n \int_0^{2\tau} dt_1 \int_0^{2\tau} dt_2 \exp(-\lambda_n D|t_2 - t_1|) g(t_1) g(t_2), \quad (3)\end{aligned}$$

where $\mathbf{g}(t) = g(t)\,\widehat{\mathbf{g}}$, $\widehat{\mathbf{g}}$ is a unit vector along the gradient direction and

$$B_n = \int_V d\mathbf{r}_1 \int_V d\mathbf{r}_2\, \widehat{\mathbf{g}}\,\mathbf{r}_1\,\widehat{\mathbf{g}}\,\mathbf{r}_2 u_n(\mathbf{r}_1) u_n(\mathbf{r}_2). \quad (4)$$

B_n and λ_n are structure dependent coefficients. For example, for diffusion between two impermeable planes separated by a distance d,

$$B_n = \frac{8d^2}{(2n-1)^4\pi^4} \text{ and } \lambda_n = \frac{\pi^2(2n-1)^2}{d^2}. \quad (5)$$

For diffusion inside an impermeable cylindrical geometry with a radius R and gradients in the direction perpendicular to the axis of the cylinder,

$$B_n = \frac{2(R/\mu_n)^2}{\mu_n^2 - 1} \text{ and } \lambda_n = \left(\frac{\mu_n}{R}\right)^2. \quad (6)$$

Here μ_n is the nth root of $J_1'(\mu) = 0$ and J_1 is a Bessel function of the first kind. For a spherical geometry, the expression for B_n is

$$B_n = \frac{2(R/\mu_n)^2}{\mu_n^2 - 2}, \quad (7)$$

and λ_n are the same as for a cylindrical geometry except μ_n becomes the nth root of $\mu J_{3/2}'(\mu) - \frac{1}{2}J_{3/2}(\mu) = 0$ [24]. For diffusion inside an impermeable spherical shell ($a < r < b$), the expression for B_n is

$$B_n = \frac{2a^3b^3[j_1'(\lambda_n a) - j_1'(\lambda_n b)]^2}{\lambda_n^2(b^3 - a^3)\{a^3(\lambda_n^2 b^2 - 2)j_1'^2(\lambda_n a) - b^3(\lambda_n^2 a^2 - 2)j_1'^2(\lambda_n b)\}}. \quad (8)$$

The detailed explanation of Eq. (8) and the corresponding conditional probability function are given in Appendix A.

2.2. Modeling DW signals with OGSE

Based on the theory introduced above, we have derived analytical expressions for the DW echo attenuation for restricted diffusion with two commonly used OGSE waveforms, cos-OGSE and sin-OGSE. The effective diffusion gradient of the cos-OSGE method has a cosine-modulated waveform as

$$g(t) = \begin{cases} G\cos[\omega t] & 0 < t < \sigma \\ -G\cos[\omega(t-\tau)] & \tau < t < (\tau + \sigma) \\ 0 & \text{else} \end{cases}, \quad (9)$$

while the sin-OGSE method uses

$$g(t) = \begin{cases} G\sin[\omega t] & 0 < t < \sigma \\ -G\sin[\omega(t-\tau)] & \tau < t < (\tau + \sigma) \\ 0 & \text{else} \end{cases}. \quad (10)$$

Here G is the gradient amplitude, ω the diffusion gradient angular frequency, σ is the gradient duration, τ half of the echo time. By substituting Eq. (9) and Eq. (10) into Eq. (3), an analytical expression for signal echo attenuation can be obtained after a straightforward derivation. For the cosine-modulated waveform,

$$\beta(2\tau) = 2(\gamma g)^2 \sum_n \frac{B_n \lambda_n^2 D^2}{(\lambda_n^2 D^2 + \omega^2)^2} \left\{ \frac{(\lambda_n^2 D^2 + \omega^2)}{\lambda_n D} \left[\frac{\sigma}{2} + \frac{\sin(2\omega\sigma)}{4\omega} \right] - 1 + \exp(-\lambda_n D\sigma) + \exp(-\lambda_n D\tau)(1 - \cosh(\lambda_n D\sigma)) \right\} \quad (11)$$

while for the sin-OGSE waveform

$$\beta(2\tau) = 2(\gamma g)^2 \sum_n \frac{B_n \omega^2}{(\lambda_n^2 D^2 + \omega^2)^2} \left\{ \frac{\lambda_n D\sigma(\lambda_n^2 D^2 + \omega^2)}{2\omega^2} + 1 - \exp(-\lambda_n D\sigma) - \exp(-\lambda_n D\tau)(1 - \cosh(\lambda_n D\sigma)) \right\}. \quad (12)$$

Here D is the intrinsic diffusion coefficient. The connection of Eq. (11) with previously published analytical DW signal models, including the PGSE models, can be found in Appendix B. Note that the b value of cos-OGSE is [27]

$$b = \frac{\gamma^2 G^2 \sigma}{4\pi^2 f^2}. \quad (13)$$

The frequency-domain analysis shows that, ideally, the cos-OGSE has a well defined frequency and corresponds to a single diffusion time [22,25], which simplifies the interpretation of OGSE measurements. Therefore, the cos-OGSE waveform and Eq. (11) are used throughout the rest of this work.

The analytical expressions can be compared to the predictions of computer simulations of diffusion in simple systems. We have previously reported our method for simulating diffusion using a finite difference approach [28] and this has been applied to predict the behaviors of OGSE measurements in tissues. We show how it is then feasible to fit such data using the analytical expressions shown above and to extract quantitative structural parameters of the media.

3. Methods

3.1. Diffusion between two parallel planes

First, the elementary case of diffusion between two infinitely large impermeable parallel planes using the cosine OGSE waveform was studied. This model illustrates the major physical effects of restricted diffusion and how these interact with the OGSE parameters. The DW signal echo attenuation was simulated as described below and then compared with the analytical results predicted by Eq. (11). A one-dimensional gradient was considered perpendicular to the planes and the distance between the planes was 10 μm, corresponding to a typical human cell size. Five diffusion gradient frequencies (100, 500, 1000, 2000 and 3000 Hz) were considered, each using 13 b values (11 values ranged evenly from 0 to 5000 mm^2/s and two additional b values of 100 mm^2/s and 300 mm^2/s to show signal variations at low b values). The simulation used spatial resolution Δx = 0.1 μm, time increment Δt = 1 μs and diffusion coefficient D = 2.0 μm^2/ms.

3.2. Cylindrical array

Axons have often been modeled as cylinders [29–32] and white matter may be considered as an array of two compartment cylinders in which components with short T_2 (e.g., myelin water) are treated as negligible in the simulation due to the relatively long experimental echo times. As suggested by Ford and Hackney [30], cylinders were placed on a square lattice to simulate healthy white matter (see Fig. 1). The diffusion gradients are perpendicular to the axis of cylinders. It has been reported that the water exchange between axons and extracellular space is intermediate or slow [33] and so the interface permeability was set equal to zero. There are then two diffusion

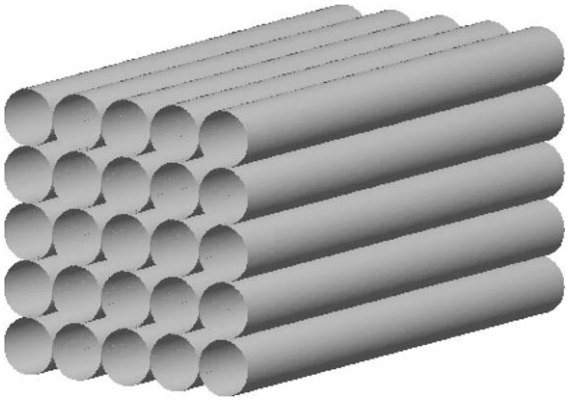

Fig. 1. Healthy white matter tissues are modeled as a cylindrical array with an arrangement of square lattice.

modes in this system: restricted diffusion inside the axon and hindered diffusion in the extracellular space [32]. The total signal echo attenuation from such a model tissue is then simply the sum of the signals arising from the two compartments

$$E = f_{axon} \exp(-\beta(2\tau)) + (1 - f_{axon}) \exp(-bD_{ex}), \quad (14)$$

where $\beta(2\tau)$ is the signal echo attenuation of water inside axons, D_{ex} is the hindered diffusion coefficient of extracellular space, and f_{axon} is the volume fraction of axons. β can be obtained from Eq. (11) with structural parameters introduced in Eq. (6). It should be noted that the signal from extracellular space is described as a mono-exponential function, so a Gaussian approximation has been assumed [34].

In the simulation, the intra- and extra-cellular intrinsic diffusion coefficients are assumed to be 1.00 and 2.00 μm^2/ms, respectively. The cylinders have a diameter of 1.96 μm, similar to a typical human axon size, and the spacing of the lattice is 2.1 μm, yielding a cylinder volume fraction 75.25%. The total signal echo attenuation was simulated and then fit to Eq. (14). All pulse sequence parameters used in the simulation were chosen to be experimentally practical values, such as b values (11 values, ranging evenly from 0 to 500 s/mm^2) and four gradient frequencies (100, 250, 500 and 1000 Hz) with TE = 40 ms. Again, Δx = 0.1 μm, Δt = 1 μs and a unit cell only was needed to be simulated [28], using a matrix of 20 × 20 elements.

To study the sensitivity of fitting the OGSE data to the presence of noise inherent in the diffusion measurements, the statistical properties of the fitted parameters obtained from our model, such as axon radius, were analyzed by adding different levels of background noise to the simulated data. This was implemented using the method proposed by Pierpaoli and Basser [35].

3.3. A 3D three-compartment tissue model

Cell size and cell density are important features of biological tissues, while the dimensions of sub-cellular structures such as the nucleus are also informative as potential biomarkers for diagnostic purposes or for characterizing the status of tumors [36]. In order to make diffusion measurements sensitive specifically to features such as nuclear size, the diffusion times incorporated into the measurements must be much shorter than those in common PGSE methods. We have previously reported that the cos-OGSE method can be sensitive to variations in intracellular structure, which are otherwise barely detectable by conventional PGSE methods [16]. However, in order to describe tissue microstructure more quantitatively and to be able to derive values for features such as cell nuclear size, an appropriate tissue model and analytical DW signal expressions must be developed.

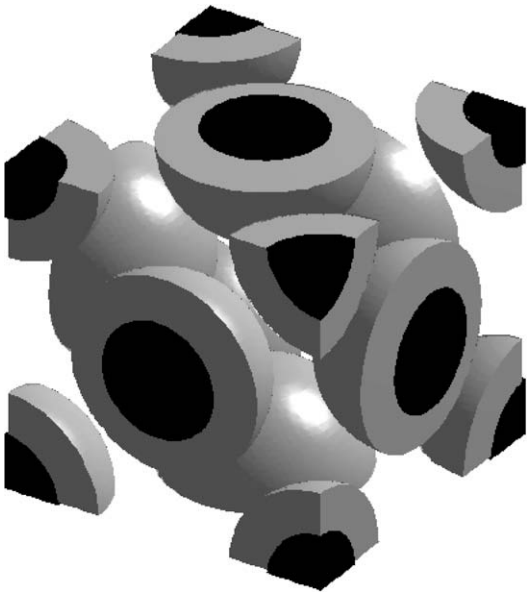

Fig. 2. A 3D multiple-compartment tissue model. Black regions are cell nuclei, gray are cytoplasm and extracellular space everywhere else. All cells are packed on a face centered cubic (FCC) lattice and a unit cell is shown here. Note that cells are shown apart than the real arrangement for visual purpose.

Fig. 2 shows a three-compartment three-dimensional tissue model consisting of spherical cells packed on a face centered cubic (FCC) lattice. Each cell contains a central spherical nucleus. As a result, there are three distinct compartments containing water in this model, corresponding to intra-nuclear, cytoplasmic and extracellular spaces. Each component in this model can be ascribed its own intrinsic parameters, including proton density, T_2 and water self-diffusion coefficient. However, proton density and T_2 values were assumed to be homogeneous in order to highlight the effects of diffusion. For the OGSE method, the effective diffusion time is on the order of the period of gradient oscillations [27], which can be smaller than a few milliseconds (corresponding to gradient frequencies higher than a few hundreds of hertz). In contrast, the intracellular water exchange lifetime has been reported to be two orders of magnitude larger, e.g., the HeLa cell intracellular water lifetime was estimated to be 119 ± 14 ms [37]. Therefore, we can neglect the influence of the water exchange between intra- and extra-cellular spaces during the OGSE measurements. For the nuclear envelope separating intra-nuclear and cytoplasmic compartments, there is not sufficient experimental data to describe the effects of water exchange on apparent diffusion at short time scales; however, we can estimate the exchange influence in our OGSE measurements. Water exchange across the nuclear envelope is by diffusion through nuclear pores [38]. The nuclear pore surface density is $\sim 10\ \mu m^{-2}$ for human cells [39] and the effective radius of each pore for Fick diffusion is 20 nm [40]. Thus, typically the surface fraction of pores is ~1.3% which means a water molecule that encounters the nuclear envelope has a probability ~0.013 to cross. For typical cell sizes and diffusion coefficients as described below, if the effective diffusion time is <2 ms, only the spins inside spherical shells with thickness <2.3 μm (in the nucleus) and <1.4 μm (in the cytoplasm) are considered likely to encounter the nuclear envelope. Hence, less than 2% of spins in the intra-nucleus or cytoplasm will exchange during a short diffusion time <2 ms. Therefore, water exchange across the nuclear envelope can be ignored in OGSE measurements with short diffusion times. If the effective diffusion time becomes long, as in conventional PGSE measurements, this approximation is no longer valid and the water exchange effect across the nuclear envelope must be considered. Consequently, all the interfaces between the compartments in the tissue model can be effectively modeled as impermeable if the OGSE method is implemented with relatively high gradient frequencies. As a result, the total signal can be modeled as a sum of independent signals, each arising from one compartment.

The diffusion inside the intra-nuclear and cytoplasmic spaces is considered to be restricted, and the diffusion in the extracellular space was modeled as hindered and ascribed a constant diffusion coefficient. The total DW signals can then be expressed as

$$E = f_{nuc}\exp(-\beta_{nuc}) + f_{cyto}\exp(-\beta_{cyto}) + (1 - f_{nuc} - f_{cyto})\exp(-bD_{ex}), \quad (15)$$

where β_{nuc} and β_{cyto} represent the signal echo attenuation of intra-nuclear and cytoplasmic spaces, respectively, and f_{nuc}, f_{cyto} represent proton fractions (equal to volume fractions because proton density is assumed to be homogeneous). Therefore, there are six independent fitting parameters in Eq. (15); R_{nuc} and R_{cell} are the radii of nuclei and cells, respectively; D_{nuc}, D_{cyto} and D_{ex} are the diffusion coefficients of the three compartments; and f_{nuc} is the volume fraction of nuclei. The volume fraction of cytoplasm f_{cyto} is a dependent parameter which can be expressed as $f_{cyto} = f_{nuc}(R_{cell}/R_{nuc})^3 - f_{nuc}$.

The signal echo attenuation was simulated and then fit to Eq. (15). All cell structural parameters used in the simulation were chosen from published experimental results [41,42]: the intrinsic diffusion coefficients for nucleus = 1.31 μm^2/ms, cytoplasm = 0.48 μm^2/ms and the extracellular space = 1.82 μm^2/ms. Spherical cells were given a diameter of 10 μm, spacing 10.6 μm for neighboring cells and each cell contained a central spherical nucleus with a diameter of 7.5 μm. All pulse sequence parameters were experimentally practical values, such as b values (11 values, ranging evenly from 0 to 500 s/mm^2) and three gradient frequencies (250, 500 and 1000) with TE = 40 ms. A 3D grid of $60 \times 60 \times 60$ elements with $\Delta x = 0.25$ μm, $\Delta t = 2$ μs was simulated. The sensitivity of the fitting OGSE data to the presence of noise was also studied.

3.4. Finite difference simulations and data fitting

An improved finite difference method [28] was used for the simulations to calculate the evolution of the diffusion-weighted NMR signals. It includes a revised periodic boundary condition that removes the computational edge effect artifact found using conventional finite difference methods and employs parallel computing to enhance the computing efficiency. Further details of the computational aspects of our method have been reported previously [28]. All large-scale simulations were performed on the supercomputer of the Vanderbilt University Advanced Computing Center for Research & Education. The programs were written in C (GCC 4.1.2) with message passing interface (MPICH2) running on a 64-bit Linux operation system and Opteron processor (2.0 GHz) nodes with a Gigabit Ethernet network. Plane and cylindrical array simulations were performed on a single processor while the 3D simulation was performed with parallel computing using eight processors.

All simulated data with and without noise were analyzed with a nonlinear regression routine (employing the Levenberg–Marquardt minimization algorithm) using MATLAB R2008a (Mathworks, Natick, MA).

4. Results

Fig. 3 compares the simulated and analytical signal echo attenuations for restricted diffusion between two infinitely large impermeable planes. The effective diffusion time monotonically decreases with increasing diffusion gradient frequency, so the sig-

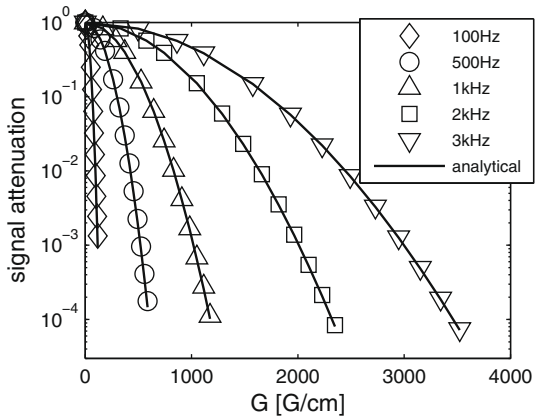

Fig. 3. Comparison of simulated (markers) and analytical (lines) signal echo attenuation of restricted diffusion between two infinitely large impermeable planes.

nal echo attenuation curves vary for different frequencies. For a certain gradient amplitude, the b value decreases when the gradient frequency increases, so the signal is more attenuated for a lower frequency at the same gradient amplitude.

The simulated and analytical signal echo attenuations shown in Fig. 3 agree well but do not match exactly. A small discrepancy can be found at higher gradient amplitudes and lower gradient frequencies. For example, at $f = 3$ kHz, the percentage difference of the simulated and analytical signals increases from 0% to 2.9% when the b values increase from 0 to 5000 mm^2/s. This may be because Eq. (1) invokes a Gaussian approximation to the signal attenuation, which ignores the contribution of the spin phase shift distribution to the signal echo attenuation and it may deviate from the true values at long diffusion times and/or high diffusion-weighting [43]. However, for realistic b values used in practice, our analytical expressions are close to unbiased. For commonly used b values in the OGSE measurements (<3000 s/mm^2), the analytical signal yields only a 2% deviation from simulated data at moderately high frequencies. Thus, the analytical expressions for the OGSE signal echo attenuation introduced above are valid for realistic b values, moderate and high gradient frequencies.

Fig. 4 shows the simulated signal echo attenuation without noise (markers) of the cylinder array shown in Fig. 1. Eq. (14) was used to fit all simulated data. The fitted structural parameters and the corresponding values used in simulations are shown in Table 1, in which R is the radius of axon, D_{in} and D_{ex} are diffusion coefficients of axons and extracellular space, respectively. As expected,

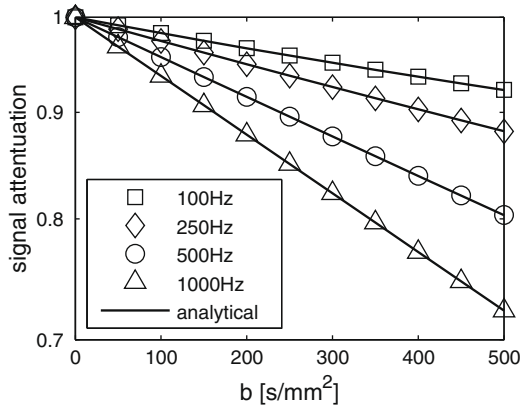

Fig. 4. Simulated signal echo attenuation (markers) of modeled white mater tissue (shown in Fig. 1). Solid lines are corresponding fitted curves.

Table 1
Comparison of real structural parameters used in simulations and fitted parameters for the cylindrical array.

	R (μm)	D_{in} (μm^2/ms)	D_{ex} (μm^2/ms)	f_{axon} (%)
Real value	0.98	1.00	2.00	75.25
Fitted value	0.99	1.00	0.69	76.79

the fitted extracellular diffusion coefficient D_{ex} is smaller than the intrinsic value because the extracellular space is modeled as showing hindered diffusion and the fitted D_{ex} is actually a hindered diffusion coefficient, representing the averaged effects of obstruction by the barriers. All of the other fitted parameters have less than 1% difference.

To comprehensively study the influence of the signal-to-noise ratio (SNR) on the fitted parameter of the analytical model presented in the current work, background noise of different levels was added to the simulated signals, and then the fitting was repeated 5000 times for each SNR. Fig. 5 shows the distribution of the fitted axon radii changes with SNR. At SNR = 50, the fitted axon radii ranges from 0.8 to 1.8 μm with a peak at 0.9 μm, corresponding to an error range −20% to 80%. At SNR = 800, >99% fitted axon radii have less than 5% error.

Fig. 6 shows the comparison of the simulated (without noise) and fitted signal attenuation for the three-dimensional three-compartment tissue model illustrated in Fig. 2. The simulated data were fit very well by the analytical expressions, and the fitted structural parameters are listed in Table 2. All fitted parameters have less than 1% difference compared with the actual values, except the hindered diffusion coefficient D_{ex} is much lower as expected. Based on the fitted parameters shown in Table 2, the volume fractions of cytoplasm and extracellular space can be calculated as 36.00% and 37.67%, matching the actual values (35.66% and 38.15%) well.

Figs. 7 and 8 shows how fitted nuclear radii and cell radii change with SNR, respectively. Compared with the 2D model shown in Fig. 5, the 3D model is more sensitive to the noise. The fitted nuclear radii and cell radii show relatively broad ranges with low SNRs, such as when SNR = 50, 90% fitted nuclear radii are in the range [1.45 μm, 5.75 μm], corresponding to an error range [−61%, 53%]. When SNR = 800, 90% fitted nuclear radii range is [3.32 μm, 3.92 μm], corresponding to an error range [−11.5%, 4.5%].

5. Discussion

Temporal diffusion spectroscopy as described here is different from diffusion q space imaging. In the latter the propagator is usually defined at a given diffusion time and has spatial and directional dependences over a large range of q space. In contrast, in temporal diffusion spectroscopy the effective diffusion times are changed by changing diffusion gradient frequencies, and thus a spectrum of diffusion rates can be measured which describe the biological tissue microenvironment [22]. Considering the strength limitation of conventional gradient systems, the model introduced in this work does not use the whole spectrum but rather several discrete frequencies and multiple b values, but from these measurements quantitative tissue micro-structural information can be obtained.

Our model is based on Eq. (1), which is derived from a Gaussian phase approximation [34,44,45]. For conventional diffusion measurements with the PGSE method, this approximation is often violated especially at high b values with relatively long diffusion times. The OGSE method has the ability to reduce the effective diffusion time significantly so that a Gaussian approximation is still valid. Note that violating the Gaussian approximation may contribute errors and may increase the discrepancies between real and fit-

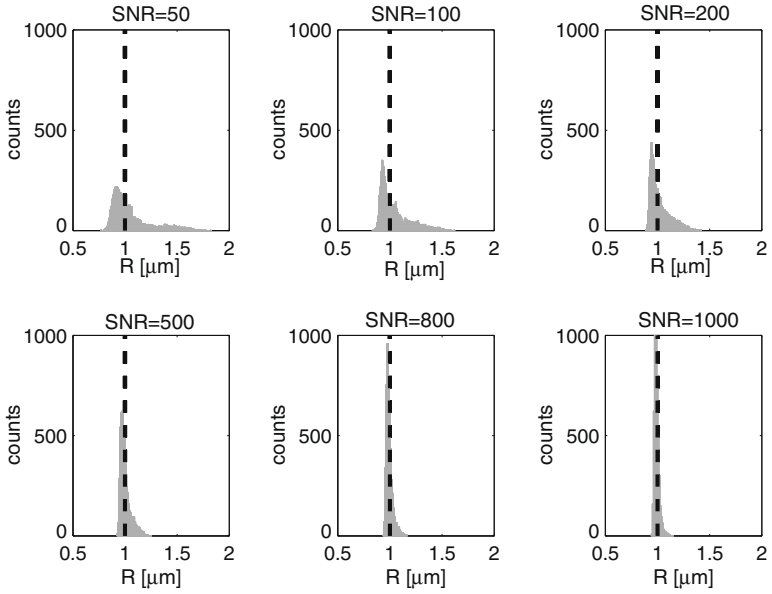

Fig. 5. For each SNR, data fitting for the cylinder array model was repeated 5000 times and the distributions of fitted axon radii changing with SNR are shown here. Dashed lines represent the real value.

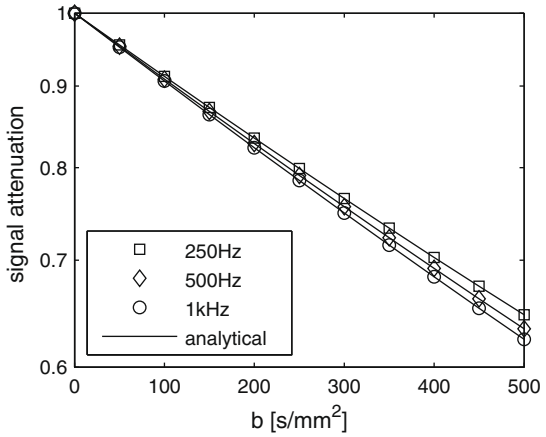

Fig. 6. Simulated signal echo attenuation (markers) of modeled 3D three-compartment tissues (shown in Fig. 2). Solid lines are corresponding fitted curves.

ted parameter values. Hence, it is prudent to apply high enough gradient frequencies in experiments so that the method introduced in the present work can be implemented accurately.

In the cylindrical array tissue model (mimicking white matter), the diffusion gradients have been assumed perpendicular to the axis of cylinders. It is also of interest to study diffusion tensor imaging (DTI) in which diffusion gradients have angular dependence with respect to fiber orientations in three dimensions. An approach similar to the CHARMD model [32], which analyzes perpendicular and parallel diffusion signals separately, might be analogously implemented to expand the current method to DTI studies, except that the current method is expected to depend on gradient frequencies significantly.

The diffusion in the extracellular space in both the 2D and 3D models is modeled as hindered diffusion with mono-exponential signal attenuation. In the long diffusion time region, the hindered diffusion coefficient can be calculated from the tortuosity of the extracellular space. For the 2D model consisting of cylinders on a square array, the tortuosity of the extracellular space can be estimated as ~9.1 using the theoretical model for diffusion in white matter developed by Sen and Basser [46], simply setting the water concentration in the axon equal to zero and the volume fraction of myelin to zero. Hence, the long time effective diffusion coefficient of the extracellular space is ~0.22 μm^2/ms which is much smaller than the fitted D_{ex} = 0.66 μm^2/ms. This again shows that a short effective diffusion time has been achieved by OGSE methods.

There are some limitations of implementing the method developed in this paper. One important factor is the diffusion gradient strength. The b value of OGSE pulse sequences is proportional to $1/f^2$ (see Eq. (13)), and σ is limited by T_2 relaxation. Hence, it is usually difficult to achieve high b values at high gradient frequencies. OGSE methods have been readily implemented *in vivo* on animal scanners [20,27], but their use on human scanners is limited by current practical gradient systems. Computer simulations show that SNR of at least several hundreds must be achieved in order to characterize tissue micro-structural information accurately, while fitting diffusion coefficients need an even higher SNR. Therefore, SNR is another crucial limiting factor affecting the application of this approach.

6. Conclusions

Novel expressions have been developed to allow the predictions of temporal diffusion spectroscopy theory to be used to interpret data obtained from OGSE measurements. Compared with other

Table 2
Comparison of real structural parameters used in the simulations and fitted parameters for the 3D three-compartment tissue model.

	R_{nuc} (μm)	R_{cell} (μm)	D_{nuc} (μm^2/ms)	D_{cyto} (μm^2/ms)	D_{ex} (μm^2/ms)	f_{nuc} (%)
Real value	3.75	5.00	1.31	0.48	1.82	26.20
Fitted value	3.72	4.97	1.30	0.47	1.41	26.33

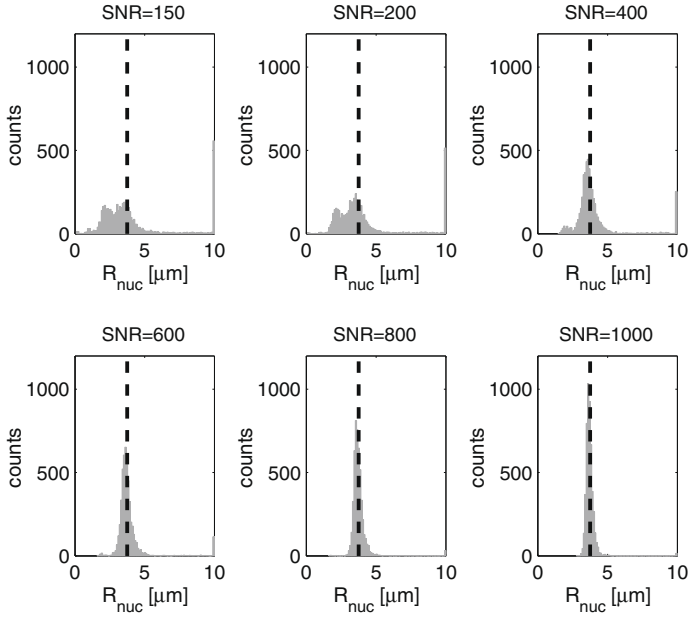

Fig. 7. For each SNR, data fitting for 3D cell-packing modeled tissue was repeated 5000 times and the distributions of fitted nuclear radii changing with SNR are shown here. Dashed lines represent the real value.

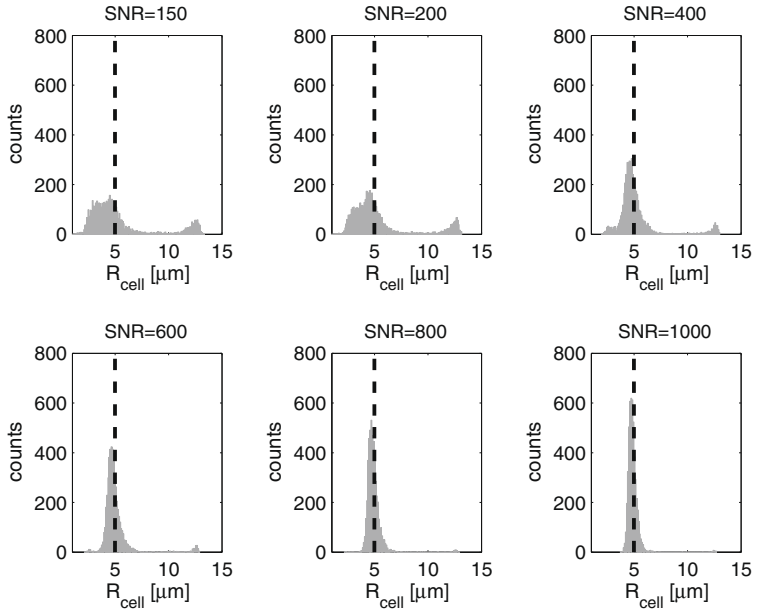

Fig. 8. The distributions of fitted cell radii of the 3D cell-packing modeled tissue changing with SNR are shown here. Dashed lines represent the real value.

models with conventional PGSE methods, this approach has the ability to extract quantitative tissue structural information, including cell nuclear sizes, which are usually not obtainable using conventional methods non-invasively. This approach provides new structural parameters which may be helpful to follow intracellular changes in tissues and potentially can be used for applications such as monitoring tumor response to treatment *in vivo*.

Acknowledgments

We thank one anonymous reviewer who pointed out a mistake in the original manuscript and whose comments have led to an improved version of this manuscript. This work was funded by NIH Grants CA109106, NS034834, EB001744 and NSF 0448915. The simulations used the resources of the Advanced Computing Center for Research and Education (ACCRE) at Vanderbilt University, Nashville, TN.

Appendix A

We derived the analytical expression of conditional probability for restricted diffusion inside an impermeable spherical shell ($a < r < b$) as

$$P(\mathbf{r}, t|\mathbf{r_0}, 0) = \frac{3}{4\pi(b^3 - a^3)} + \sum_{n=1}^{\infty}\sum_{m=1}^{\infty} A_{nm} U_n(\lambda_{nm} r) P_n(\cos\theta) \\ U_n(\lambda_{nm} r_0) P_n(\cos\theta_0) \exp(-\lambda_{nm}^2 D t), \quad \text{(A1)}$$

where

$$A_{nm}=\frac{(2n+1)\lambda_{nm}^6a^3b^3}{2\pi\left\{a^3[\lambda_{nm}^2b^2-n(n+1)]\left[\frac{j_n'(\lambda_{nm}a)}{j_n'(\lambda_{nm}b)}\right]^2-b^3[\lambda_{nm}^2a^2-n(n+1)]\right\}} \quad (A2)$$

$$U_n(\lambda_{nm}r)=y_n'(\lambda_{nm}a)j_n(\lambda_{nm}r)-j_n'(\lambda_{nm}a)y_n(\lambda_{nm}r), \quad (A3)$$

and λ_{nm} is the mth root of the equation

$$y_n'(\lambda_{nm}a)j_n'(\lambda_{nm}b)=j_n'(\lambda_{nm}a)y_n'(\lambda_{nm}b), \quad (A4)$$

where $j_n(r)=r^{-1/2}J_{n+1/2}(r)$ and $y_n(r)=r^{-1/2}Y_{n+1/2}(r)$, $J_{n+1/2}$ and $Y_{n+1/2}$ are Bessel functions of the first and the second kind, respectively.

Eq. (A1) and Eq. (4) yield the B_n coefficient as

$$B_n=\frac{2a^3b^3[j_1'(\lambda_na)-j_1'(\lambda_nb)]^2}{\lambda_n^2(b^3-a^3)\{a^3(\lambda_n^2b^2-2)j_1'^2(\lambda_na)-b^3(\lambda_n^2a^2-2)j_1'^2(\lambda_nb)\}}. \quad (A5)$$

If $a\to 0$, a spherical shell becomes a sphere and Eq. (A5) becomes identical to Eq. (7).

Appendix B

Recall Eq. (11)

$$\beta(2\tau)=2(\gamma g)^2\sum_n\frac{B_n\lambda_n^2D^2}{(\lambda_n^2D^2+\omega^2)^2}\left\{\frac{(\lambda_n^2D^2+\omega^2)}{\lambda_nD}\left[\frac{\sigma}{2}+\frac{\sin(2\omega\sigma)}{4\omega}\right]-1+\exp(-\lambda_nD\sigma)+\exp(-\lambda_nD\tau)(1-\cosh(\lambda_nD\sigma))\right\}, \quad (B1)$$

where ω is the gradient angular frequency, σ the gradient duration and τ half of the echo time. Eq. (B1) is the analytical expression for signal attenuation of cos-OGSE with restricted diffusion. When the diffusion time is short compared to the time for molecules to reach the boundary, i.e., $\frac{1}{\lambda_nD}>>\tau$, Eq. (B1) becomes

$$\beta(2\tau)=\frac{\gamma^2G^2D\sigma}{\omega^2}=\frac{\gamma^2G^2\sigma}{4\pi^2f^2}D. \quad (B2)$$

Note that the fact $\sum_nB_n\lambda_n=1$ is used. Eq. (B2) describes free diffusion with the cos-OGSE method which is equivalent to results derived in Ref. [27].

If $\omega\to 0$, a cos-OGSE pulse degenerates into a conventional PGSE pulse and Eq. (B1) becomes

$$\beta(2\tau)=2\left(\frac{\gamma g}{D}\right)^2\sum_n\frac{B_n}{\lambda_n^2}\{\lambda_nD\sigma-1+e^{-\lambda_nD\sigma}+e^{-\lambda_nD\tau}(1-\cosh(\lambda_nD\sigma))\}, \quad (B3)$$

which has been reported previously [24].

If $\tau=\sigma$, Eq. (B3) yields

$$\beta(2\tau)=\left(\frac{\gamma G}{D}\right)^2\sum_n\frac{B_n}{\lambda_n^2}[2\lambda_nD\tau-3+4\exp(-\lambda_nD\tau)-\exp(-2\lambda_nD\tau)], \quad (B4)$$

which describes the signal echo attenuation for a magnetic-field gradient pulse. Eq. (B4) has also been obtained in Ref. [47], which used a different approach.

References

[1] J.B. Hursh, Conduction velocity and diameter of nerve fibers, Am. J. Physiol. 127 (1939) 131–139.
[2] J.M. Ritchie, On the relation between fibre diameter and conduction velocity in myelinated nerve fibres, Proc. R. Soc. Lond. B Biol. Sci. 217 (1982) 29–35.
[3] Y. Assaf, T. Blumenfeld-Katzir, Y. Yovel, P.J. Basser, AxCaliber: a method for measuring axon diameter distribution from diffusion MRI, Magn. Reson. Med. 59 (2008) 1347–1354.
[4] S.C. Fang, C. de los Reyes, J.G. Umen, Cell size checkpoint control by the retinoblastoma tumor suppressor pathway, PLoS Genet. 2 (2006) e167.
[5] Y. Arai, K. Okubo, N. Terada, Y. Matsuta, S. Egawa, S. Kuwao, K. Ogura, Volume-weighted mean nuclear volume predicts tumor biology of clinically organ-confined prostate cancer, Prostate 46 (2001) 134–141.
[6] C.Y. Hsu, R.J. Kurman, R. Vang, T.L. Wang, J. Baak, M. Shih Ie, Nuclear size distinguishes low- from high-grade ovarian serous carcinoma and predicts outcome, Hum. Pathol. 36 (2005) 1049–1054.
[7] E.O. Stejskal, Use of spin echoes in a pulsed magnetic-field gradient to study anisotropic restricted diffusion and flow, J. Chem. Phys. 43 (1965) 3597–3603.
[8] P.T. Callaghan, Principles of Nuclear Magnetic Resonance Microscopy, Clarendon Press; Oxford University Press, Oxford [England]; New York, 1991.
[9] D.G. Cory, A.N. Garroway, Measurement of translational displacement probabilities by NMR: an indicator of compartmentation, Magn. Reson. Med. 14 (1990) 435–444.
[10] B. Balinov, B. Jonsson, P. Linse, O. Soderman, The NMR self-diffusion method applied to restricted diffusion – simulation of echo attenuation from molecules in spheres and between planes, J. Magn. Reson. A 104 (1993) 17–25.
[11] K.R. Brownstein, C.E. Tarr, Importance of classical diffusion in NMR-studies of water in biological cells, Phys. Rev. A 19 (1979) 2446–2453.
[12] J.E. Tanner, E.O. Stejskal, Restricted self-diffusion of protons in colloidal systems by pulsed-gradient spin-echo method, J. Chem. Phys. 49 (1968) 1768–1777.
[13] C.H. Neuman, Spin-echo of spins diffusing in a bounded medium, J. Chem. Phys. 60 (1974) 4508–4511.
[14] L. Zhao, A.L. Sukstanskii, C.D. Kroenke, J. Song, D. Piwnica-Worms, J.J. Ackerman, J.J. Neil, Intracellular water specific MR of microbead-adherent cells: HeLa cell intracellular water diffusion, Magn. Reson. Med. 59 (2008) 79–84.
[15] D.A. Yablonskiy, G.L. Bretthorst, J.J. Ackerman, Statistical model for diffusion attenuated MR signal, Magn. Reson. Med. 50 (2003) 664–669.
[16] J. Xu, M.D. Does, J.C. Gore, Sensitivity of MR diffusion measurements to variations in intracellular structure: effects of nuclear size, Magn. Reson. Med. 61 (2009) 828–833.
[17] M. Schachter, M.D. Does, A.W. Anderson, J.C. Gore, Measurements of restricted diffusion using an oscillating gradient spin-echo sequence, J. Magn. Reson. 147 (2000) 232–237.
[18] M.D. Does, E.C. Parsons, J.C. Gore, Oscillating gradient measurements of water diffusion in normal and globally ischemic rat brain, Magn. Reson. Med. 49 (2003) 206–215.
[19] M. Carl, G. Wilson Miller, J.P. Mugler 3rd, S. Rohrbaugh, W.A. Tobias, G.D. Cates Jr., Measurement of hyperpolarized gas diffusion at very short time scales, J. Magn. Reson. 189 (2007) 228–240.
[20] D.C. Colvin, T.E. Yankeelov, M.D. Does, Z. Yue, C. Quarles, J.C. Gore, New insights into tumor microstructure using temporal diffusion spectroscopy, Cancer Res. 68 (2008) 5941–5947.
[21] P.T. Callaghan, A simple matrix formalism for spin echo analysis of restricted diffusion under generalized gradient waveforms, J. Magn. Reson. 129 (1997) 74–84.
[22] E.C. Parsons Jr., M.D. Does, J.C. Gore, Temporal diffusion spectroscopy: theory and implementation in restricted systems using oscillating gradients, Magn. Reson. Med. 55 (2006) 75–84.
[23] J. Stepisnik, Analysis of NMR self-diffusion measurements by a density-matrix calculation, Physica B 104 (1981) 350–364.
[24] J. Stepisnik, Time-dependent self-diffusion by NMR spin-echo, Physica B 183 (1993) 343–350.
[25] P.T. Callaghan, J. Stepisnik, Frequency-domain analysis of spin motion using modulated-gradient NMR, J. Magn. Reson. A 117 (1995) 118–122.
[26] P.T. Callaghan, Pulsed-gradient spin-echo NMR for planar, cylindrical, and spherical pores under conditions of wall relaxation, J. Magn. Reson. A 113 (1995) 53–59.
[27] M.D. Does, E.C. Parsons, J.C. Gore, Oscillating gradient measurements of water diffusion in normal and globally ischemic rat brain, Magn. Reson. Med. 49 (2003) 206–215.
[28] J. Xu, M.D. Does, J.C. Gore, Numerical study of water diffusion in biological tissues using an improved finite difference method, Phys. Med. Biol. 52 (2007) N111–N126.
[29] A. Szafer, J. Zhong, J.C. Gore, Theoretical model for water diffusion in tissues, Magn. Reson. Med. 33 (1995) 697–712.
[30] J.C. Ford, D.B. Hackney, Numerical model for calculation of apparent diffusion coefficients (ADC) in permeable cylinders – comparison with measured ADC in spinal cord white matter, Magn. Reson. Med. 37 (1997) 387–394.
[31] S.N. Hwang, C.L. Chin, F.W. Wehrli, D.B. Hackney, An image-based finite difference model for simulating restricted diffusion, Magn. Reson. Med. 50 (2003) 373–382.
[32] Y. Assaf, R.Z. Freidlin, G.K. Rohde, P.J. Basser, New modeling and experimental framework to characterize hindered and restricted water diffusion in brain white matter, Magn. Reson. Med. 52 (2004) 965–978.
[33] Y. Assaf, A. Mayk, Y. Cohen, Displacement imaging of spinal cord using q-space diffusion-weighted MRI, Magn. Reson. Med. 44 (2000) 713–722.
[34] L.J. Zielinski, P.N. Sen, Effects of finite-width pulses in the pulsed-field gradient measurement of the diffusion coefficient in connected porous media, J. Magn. Reson. 165 (2003) 153–161.
[35] C. Pierpaoli, P.J. Basser, Toward a quantitative assessment of diffusion anisotropy, Magn. Reson. Med. 36 (1996) 893–906.
[36] D. Zink, A.H. Fischer, J.A. Nickerson, Nuclear structure in cancer cells, Nat. Rev. Cancer 4 (2004) 677–687.
[37] L. Zhao, C.D. Kroenke, J. Song, D. Piwnica-Worms, J.J. Ackerman, J.J. Neil, Intracellular water-specific MR of microbead-adherent cells: the HeLa cell intracellular water exchange lifetime, NMR Biomed. 21 (2008) 159–164.

[38] B. Talcott, M.S. Moore, Getting across the nuclear pore complex, Trends Cell Biol. 9 (1999) 312–318.
[39] G.G. Maul, L. Deaven, Quantitative determination of nuclear pore complexes in cycling cells with differing DNA content, J. Cell Biol. 73 (1977) 748–760.
[40] K. Ribbeck, D. Gorlich, Kinetic analysis of translocation through nuclear pore complexes, EMBO J. 20 (2001) 1320–1330.
[41] A.W. Anderson, J. Xie, J. Pizzonia, R.A. Bronen, D.D. Spencer, J.C. Gore, Effects of cell volume fraction changes on apparent diffusion in human cells, Magn. Reson. Imaging 18 (2000) 689–695.
[42] S.C. Grant, D.L. Buckley, S. Gibbs, A.G. Webb, S.J. Blackband, MR microscopy of multicomponent diffusion in single neurons, Magn. Reson. Med. 46 (2001) 1107–1112.
[43] J. Stepisnik, A new view of the spin echo diffusive diffraction in porous structures, Europhys. Lett. 60 (2002) 453–459.
[44] A.F. Frohlich, S.N. Jespersen, L. Ostergaard, V.G. Kiselev, The effect of impermeable boundaries of arbitrary geometry on the apparent diffusion coefficient, J. Magn. Reson. 194 (2008) 128–135.
[45] A.F. Frohlich, L. Ostergaard, V.G. Kiselev, Effect of impermeable boundaries on diffusion-attenuated MR signal, J. Magn. Reson. 179 (2006) 223–233.
[46] P.N. Sen, P.J. Basser, A model for diffusion in white matter in the brain, Biophys. J. 89 (2005) 2927–2938.
[47] B. Robertson, Spin-echo decay of spins diffusing in a bounded region, Phys. Rev. 151 (1966) 273.